

# Shock tube and modeling study of soot formation during the pyrolysis and oxidation of a number of aliphatic and aromatic hydrocarbons

G.L. Agafonov, V.N. Smirnov, P.A. Vlasov<sup>\*</sup>

*Semenov Institute of Chemical Physics, Russian Academy of Sciences, Kosygin Str. 4, 119991 Moscow, Russia*

Available online 25 September 2010

---

## Abstract

An experimental and modeling study of soot formation during the shock-tube pyrolysis and oxidation of a number of aromatic and aliphatic hydrocarbons was performed. Hydrocarbons with different chemical structures, both aliphatic (methane, propane, and propylene) and aromatic (benzene, toluene, and ethylbenzene), were tested. The experiments showed that the soot formation during the pyrolysis, even in the presence of small amounts of oxygen, is accompanied by a temperature decrease. A new, essentially modified detailed kinetic model of soot formation is proposed, which was successfully tested by describing the published data on the temporal behavior of a number of key species during the initial stages of pyrolysis and oxidation of a number of hydrocarbons under various conditions. When applied to modeling our experimental data, it closely reproduced the time profiles of the soot yield and temperature for the shock-tube pyrolysis of methane, propane, and propylene, as well as benzene, toluene, and ethylbenzene, two sets of compounds of drastically different natures.

© 2010 The Combustion Institute. Published by Elsevier Inc. All rights reserved.

**Keywords:** Soot formation; Shock tube; Pyrolysis; Oxidation; Kinetic modeling

---

## 1. Introduction

In spite of a significant progress in the experimental studies and theoretical interpretation of soot formation, some aspects of this complex process remain poorly understood. One of the effective tools for investigating soot formation is the shock-tube technique. An obvious advantage of this technique is the possibility of exactly controlling various experimental conditions, such as the temperature, pressure, and reaction mixture composition, for a few milliseconds. This makes it possible to examine the

predictive possibilities of detailed gas-phase kinetic schemes of soot formation.

The mechanism of the formation of soot particle nuclei is the central theoretical problem of soot formation; however, some aspects of the mechanism of evolution of soot nuclei into young soot particles and, further, into mature soot particles remain unclear.

Frenklach and some other authors (see, e.g., [1,2] and references therein) characterize soot particle formation as sticking of PAHs to form stacks of dimers, trimers, etc., while individual PAH species keep increasing in size via molecular chemical growth reactions. The sticking, in turn, is a merely physical process, since it is controlled by the van der Waals force, without formation of chemical bonds.

---

<sup>\*</sup> Corresponding author. Fax: +7 4956512191.  
E-mail address: [iz@chph.ras.ru](mailto:iz@chph.ras.ru) (P.A. Vlasov).

The emergence of the “solid” particle phase, i.e., inception, is believed to proceed through the formation of dimers, which are assumed to consist predominantly of pyrene molecules.

In other mechanisms, aromatic species are assumed to grow through radical-molecular reactions. An example is the mechanism proposed by Violi and her coworkers [3–7]. Its main feature is the addition of an aryl radical (e.g., naphthyl) to a double bond of a five-membered ring in PAHs, for example, acenaphthylene, followed by H abstraction from the site at which the addition took place. This restores the resonant structure, which is particularly stable. When the process is repeated, heavier molecular species are formed, which consist of small aromatic substructures composed of up to three rings held together by aliphatic bonds [4]. According to this scenario, inception occurs when the bays are closed after H abstraction, leading to an extension of the “aromatic islands” [5].

Recent experiments by Wang et al. [8] confirmed that freshly nucleated soot is primarily composed of aromatic structures. As was observed in [8], while soot nucleation and mass growth at early stages are dominated by aromatic compounds, the reaction of aliphatic species with the soot particles is an important factor at later stages of soot growth.

Based on an analysis of a 193-nm photoionization mass spectra, the authors of [9] demonstrated the simultaneous detection of two types of soot precursor particles consisting of stacks of pericondensed PAHs and PAH clusters bound via aliphatic bonds. At certain conditions and for certain fuels, even sooting flames do not yield stacked PAHs, which means that the stacking of PAHs is not the only process in soot precursor formation.

According to transmission electron microscopy, the primary soot particles consist of an inner core surrounded by a rather stable outer shell. Only the outer shell is composed of graphitic structures, which provide its stability, whereas the inner core contains relatively unstable fine particles encompassed by a carbon network.

The aim of the present work was to obtain new experimental data on soot formation during the pyrolysis and oxidation under rich conditions of hydrocarbons of drastically different types: aliphatic (methane, propane, and propylene) and aromatic (benzene, toluene, and ethylbenzene) and to interpret them within the framework of a kinetic model in order to elucidate whether there exists a single mechanism suitable for describing soot formation in systems of different types [10].

## 2. Experimental

The experiments were performed using a shock tube equipped with a variety of spectroscopic

facilities for monitoring the process of soot formation [11,12].

The parameters of the gas behind the reflected shock wave were calculated from the incident shock velocity and the composition of the test mixture by using the ideal-flow shock-tube theory. The distance from the endplate to the observation section was 15 mm. Briefly, the soot yield was calculated by the formula

$$SY = \frac{1}{\alpha I [C_{total}] E(m)} \ln \left( \frac{I_0}{I} \right) \quad (1)$$

Here,  $\alpha$  is the absorption coefficient (in our case,  $\alpha = 1.92 \times 10^6 \text{ cm}^2/\text{mol}$ ),  $I$  is the shock-tube diameter (cm),  $[C_{total}]$  is the total concentration of carbon atoms in the system ( $\text{mol}/\text{cm}^3$ ),  $I_0$  and  $I$  are the intensities of the incident and transmitted light (mV), and  $E(m)$  is the dimensionless absorption function given by

$$E(m) = -\text{Im} \left( \frac{m^2 - 1}{m^2 + 2} \right) \quad (2)$$

where  $m$  is the complex refractive index. Studying the formation of soot during the pyrolysis of toluene behind reflected shock waves over a wide range of compositions, we estimated  $E(m)$  as 0.37, in close agreement with the recent data [13,14]. This value has the advantage that it was determined under conditions similar to those used in the present experiments.

The temperature of soot particles was determined as described in [11,12]. The method is based on a comparison of the radiances of the ensemble of soot particles and a calibration tungsten band lamp. The working formula for determining the temperature of soot particles reads as [11,12]

$$T_s = T_{bl} \left\{ 1 + \frac{k T_{bl} \lambda}{hc} \ln \left[ \frac{1}{S_r} \left( 1 - \frac{I}{I_0} \right) \right] \right\}^{-1} \quad (3)$$

where  $T_{bl}$  is the brightness temperature of the band lamp (K),  $k$  is the Boltzmann constant ( $1.38 \times 10^{-16} \text{ erg/K}$ ),  $h$  is the Planck constant ( $6.625 \times 10^{-27} \text{ erg-s}$ ),  $\lambda$  is the emission wavelength ( $6.328 \times 10^{-5} \text{ cm}$ ),  $c$  is the speed of light ( $3 \times 10^8 \text{ cm/s}$ ),  $S_r = S_{\text{soot emission}}/S_{\text{band lamp}}$ , is the ratio of the emission signals from the soot particles and band lamp ( $S_{\text{soot emission}}$  and  $S_{\text{band lamp}}$ , are in mV) and  $I_0$  and  $I$  are the intensities of incident light and light passed through the soot-containing medium (in mV).

Typical absorption and emission signals and the time profiles of the soot yield and temperature calculated from them are presented in Fig. 1 for toluene/Ar,  $\text{CH}_4/\text{Ar}$ ,  $\text{CH}_4/\text{O}_2/\text{Ar}$ ,  $\text{C}_3\text{H}_8/\text{Ar}$  and  $\text{C}_3\text{H}_6/\text{Ar}$  mixtures. Soot formation from methane demonstrates the longest induction period, since the pathway from methane to soot precursors for methane is longer in comparison with that for propane and, especially, for toluene, which exhibits a markedly shorter induction period.

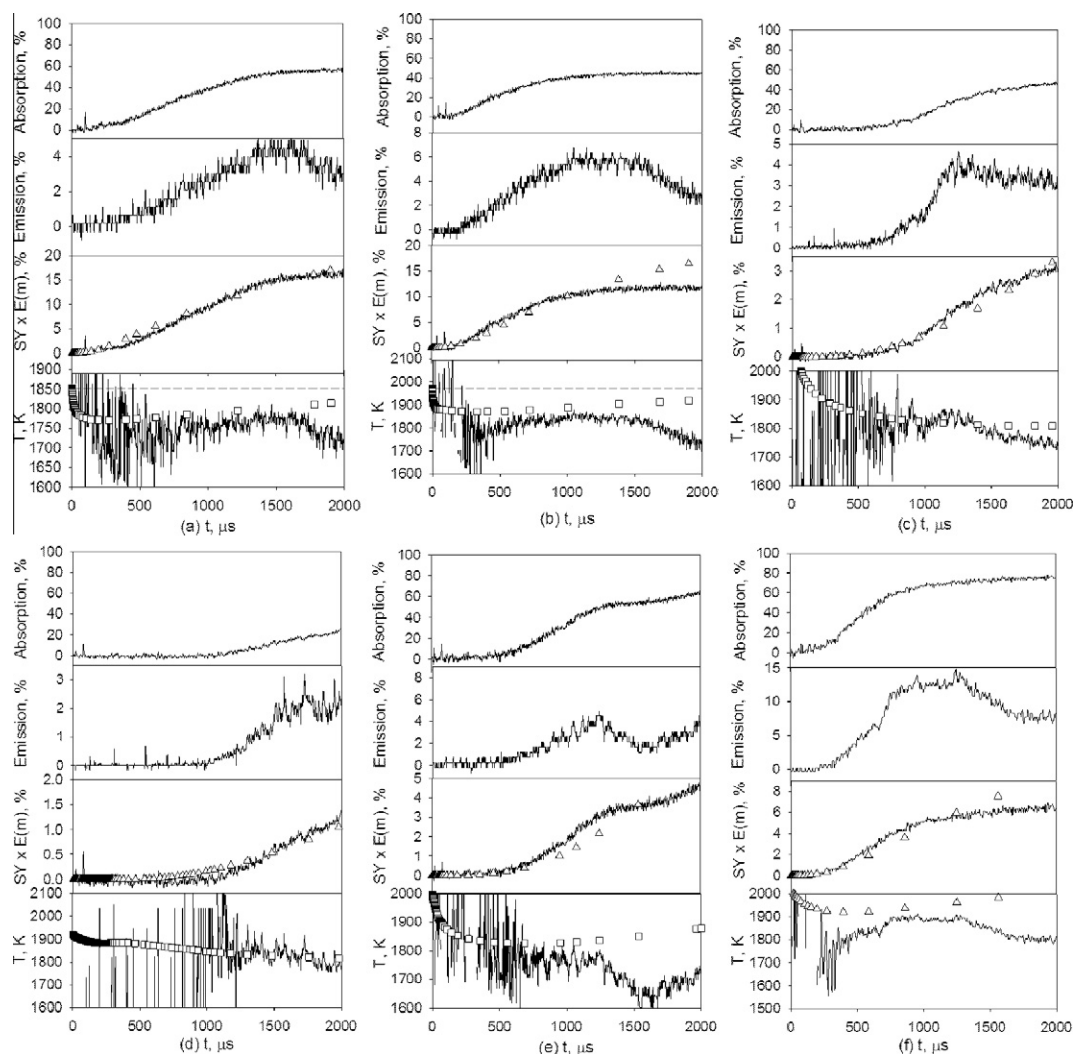


Fig. 1. Typical absorption and emission signals and time dependences of the soot yield and temperature obtained from them (a and b) for a 0.25% toluene/Ar mixture and (a)  $T_{50} = 1852$  K,  $[M]_5 = 1.96 \times 10^{-5}$  mol/cm<sup>3</sup>,  $p_{50} = 2.98$  bar, (b)  $T_{50} = 1970$  K,  $[M]_5 = 1.93 \times 10^{-5}$  mol/cm<sup>3</sup>,  $p_{50} = 3.12$  bar, (c) for a 5%CH<sub>4</sub>/Ar mixture,  $T_{50} = 2212$  K,  $[M]_5 = 2.77 \times 10^{-5}$  mol/cm<sup>3</sup>,  $p_{50} = 5.0$  bar, (d) for a 5%CH<sub>4</sub>/1.1%O<sub>2</sub>/Ar mixture,  $T_{50} = 2212$  K,  $[M]_5 = 2.77 \times 10^{-5}$  mol/cm<sup>3</sup>,  $p_{50} = 5.0$  bar, (e) for a 0.0166C<sub>3</sub>H<sub>8</sub>/Ar mixture,  $T_{50} = 2218$  K,  $[M]_5 = 2.99 \times 10^{-5}$  mol/cm<sup>3</sup>,  $p_{50} = 5.44$  bar, and (f) for a 0.0166C<sub>3</sub>H<sub>8</sub>/Ar mixture,  $T_{50} = 2210$  K,  $[M]_5 = 3.00 \times 10^{-5}$  mol/cm<sup>3</sup>,  $p_{50} = 5.44$  bar, wavelength  $\lambda = 632.8$  nm. The emission signal is given in percent with respect to the signal from the calibration band lamp. The time evolution of the soot yield and temperature were calculated under the standard assumptions: the soot particles are spherical and their optical properties are described by the Rayleigh law (the particle size is much smaller than the probing light wavelength). Triangles in frames 3 and squares in frames 4 demonstrate the calculated soot yield and gas temperature, while the curves in these frames were calculated from oscillograms given in frames 1 and 2, respectively.

The temperature drop behind the reflected shock wave front is also clearly seen even for a 0.25% toluene/Ar mixture. Therefore, all calculations in the present work were performed under nonisothermal constant-density conditions.

Note that apparent strong oscillations within the initial portion of the temperature time history in frames 4 of Fig. 1 are associated with the fact that the amplitude of noises in the absorption

and mainly emission signals are comparable with or even larger than the signals themselves; therefore, these oscillations and the temperature behavior within this time interval should be ignored as an artifact. That the emission signal drops after 1500  $\mu$ s is associated with the arrival of the rarefaction wave to the measurement section.

Our experimental results for soot formation from toluene are in close agreement with the data

obtained in [15,16] in both the induction periods and temperature dependences of the soot yield, which is indicative of the reliability of our experimental data.

### 3. Kinetic model

The kinetic mechanism was compiled as outlined in our previous works [10,11]. Similar principles were used in [18] for constructing a new chemical mechanism for the high-temperature combustion of engine fuels, ranging from methane to isooctane, with emphasis on soot precursor (benzene) formation.

In the development of such large chemical models, it is crucial to ensure the self-consistency of the rate parameters, thermochemical data, and various model assumptions. The present chemical model is based on several kinetic mechanisms, each validated for a certain group of species [17,23–25]. Combining these different models requires great care, since the rate parameters and thermochemical data for identical species and reactions may turn out to be different. The mechanism proposed in [17] for small hydrocarbons, such as methane ( $\text{CH}_4$ ) and  $\text{C}_2$ – $\text{C}_4$  species, was extended to include reactions for  $\text{C}_5$  and  $\text{C}_7$  species [23,24]. Finally, reactions involving aromatic species (benzene and toluene, [23,31]) and large alkanes (*n*-heptane, [25]) were added. When the mechanism was extended to include the reactions of larger molecules, only species and reactions not included before were added. Although this procedure does not ensure full consistency between the parameters of the model, it undoubtedly improves the predictive possibilities of the kinetic model. No reaction rates in the combined gas-phase mechanism have been changed to fit the model predictions to the experimental data.

Since the resultant mechanism involves species and reactions that have already been included in the different submechanisms, it is necessary to apply certain rules to compiling the kinetic scheme. More specifically, any species or reactions not present in the current mechanism were simply added. Additionally, when identical reactions were available, the reactions present in the current mechanism were preferred over those from the constituent submechanisms.

A new element of the mechanism used in the present work was that the core set of reactions, previously borrowed from [21], was replaced by the mechanism developed by Hai Wang and co-authors [17]. The thermal data file was also based on that given in [17]; for the species absent in [17], the thermodynamic data were taken from the other submechanisms included in the present mechanism [23–25].

The submechanism borrowed from [17] introduces a number of new reaction pathways, most importantly those involving vinylidene. At

the same time, the mechanism was extended to include a number of additional channels of PAH formation and growth (up to coronene) and a set of reactions involving  $\text{C}_3$ ,  $\text{C}_5$ , and  $\text{C}_7$  hydrocarbons [23,24]. More specifically, the mechanism included (1) the alternating H-abstraction/ $\text{C}_2\text{H}_2$ -addition (HACA) pathway, resulting in a gradual growth of PAHs; (2) the combination reactions of phenyl with  $\text{C}_6\text{H}_6$ ; (3) the cyclopentadienyl recombination; and (4) the ring-closure reactions of aliphatic hydrocarbons.

Since alkylperoxy chemistry is important at low and medium temperatures, reactions related to the formation of methylperoxy ( $\text{CH}_3\text{O}_2$ ), ethylperoxy ( $\text{C}_2\text{H}_5\text{O}_2$ ), and propylperoxy ( $\text{C}_3\text{H}_7\text{O}_2$ ) were introduced to describe the ignition delay time for  $\text{CH}_4/\text{O}_2/\text{Ar}$  mixtures [26].

The modified gas-phase reaction mechanism consists of 3320 direct and reverse reactions involving 274 species, with the rate coefficients of some important reactions being pressure-dependant.

According to our soot formation model, soot nuclei are PAHs formed by reactions between small saturated PAHs and PAH radicals or between PAH radicals alone. The reactions of formation of soot nuclei are assumed to be irreversible. The reactions of surface growth of nuclei were postulated to occur at active sites formed in reactions with hydrogen atoms. Thus, two different ensembles of soot nuclei are considered, with and without active sites.

We examined two different approaches to describing the surface growth of soot particles: the surface HACA (H-abstraction/ $\text{C}_2\text{H}_2$ -addition) model [19] and the surface growth model proposed by Harris [20].

The HACA surface mechanism is based on the assumption that the H-abstraction/ $\text{C}_2\text{H}_2$ -addition (HACA) reaction sequence is responsible for high-temperature growth of all forms of carbonaceous materials. To improve the fit between the calculated and measured soot yield time profiles, the dependences of the reactive surface fraction on the temperature and particle size determined under flame conditions [21] should be adapted to shock-tube conditions.

The Harris model of surface growth is based on the following assumptions: (1) surface growth occurs primarily on active sites, such as defects or edges; (2) the number of active sites is not directly affected by coagulation, surface growth, or gas-phase chemistry (this is a key point of the Harris model); and (3) the surface growth rate decreases because active sites are lost in the course of a temperature-dependent annealing process. Our calculations within the framework of the above surface growth model, even without regard for the annealing process, gave encouraging results.

According to our mechanism, soot nuclei are formed by radical–molecular reactions of various

PAHs, starting from phenylacetylene and acenaphthalene and ethynylnaphthalene to coronene and by radical–radical reactions (from cyclopentaphenanthrene to coronene radicals). These reactions produce polyaromatic molecules containing from 16 to 48 carbon atoms, which are stabilized by the formation of new chemical bonds. Soot nuclei are activated in reactions with H and OH radicals and deactivated in reactions with H,  $H_2$ , and  $H_2O$ . Soot nuclei grow by reacting with  $C_2H_2$ ,  $C_4H_2$ , and  $C_6H_2$  (species present at relatively high concentrations during the pyrolysis and oxidation of aliphatic and aromatic hydrocarbons) and with polyaromatic molecules and radicals, as well as with each other (coagulation). Soot nuclei are oxidized by O and OH radicals. They are transformed into soot particles via reactions of internal conversion. Soot particles grow by reacting with  $C_2H_2$ ,  $C_4H_2$ ,  $C_6H_2$  and PAH molecules and radicals. Soot particles participate in coagulation. Oxidation of soot particles is described by reactions with O and OH radicals [10].

The main difference of the gas-phase mechanism developed in the present work from the mechanism proposed in our previous studies [28,29] is that it includes a new submechanism of ethylene and acetylene combustion, developed by Hai Wang and co-authors [17], and a new set of reactions of polyene hydration followed by the decomposition of the products to smaller hydrocarbons [30,31]. Higher polyynes ( $C_{10}H_2$  and  $C_{12}H_2$ ) were excluded from the kinetic scheme. Taking into account the experiments presented in [27], the polyene submechanism of soot precursor formation proposed in [28] was not included in the present soot formation model.

The formation, growth, oxidation, and coagulation of soot nuclei and soot particles are

described using the discrete Galerkin technique [22].

#### 4. Results and discussion

The kinetic model considered was tested to simulate the time profiles of H atoms formed during the shock-tube pyrolysis of benzene [32] and phenol [33], the time profiles of OH radicals produced by the oxidation of toluene and *n*-heptane behind reflected shock waves [34], and the time profiles of  $CH_3$  radicals formed during  $C_2H_4$  thermal decomposition [35]. The results obtained in the present paper differ only slightly from those reported in [10]. The results of calculations were also compared with the experimental measurements of the main gas-phase species during shock-tube pyrolysis of a toluene/neon mixture [36], a benzene/neon mixture [37], a benzene/Ar mixture [38],  $0.02CH_4/Ar$  and  $0.05CH_4/Ar$  mixtures (Fig. 2) [39], and a  $0.016C_3H_8/Ar$  mixture [40].

As can be seen from Fig. 2, the kinetic model developed closely describes the temporal behavior of the main gas-phase species formed during methane pyrolysis. Hidaka [39] experimentally showed that the main products of the thermal decomposition of methane at high temperatures are  $C_2H_2$  and  $C_2H_4$ . Small amounts (below 1%) of  $C_2H_6$ , *p*- $C_3H_4$  (propyne), *a*- $C_3H_4$  (allene), and  $C_4H_2$  were also detected. Methane pyrolysis yields considerable amounts of methyl radicals. A reaction flow analysis of our kinetic scheme showed that, depending on the conditions, the reactions of methyl radicals produce  $C_2H_6$ ,  $C_2H_5$ , and  $C_2H_4$ , with  $C_2H_4$  being later converted into  $C_2H_3$  and  $C_2H_2$ . The reaction of  $C_2H_2$  with  $CH_3$  gives propyne *p*- $C_3H_4$ , which, in turn, produces allene *a*- $C_3H_4$ . Propyne, allene, and acetylene are

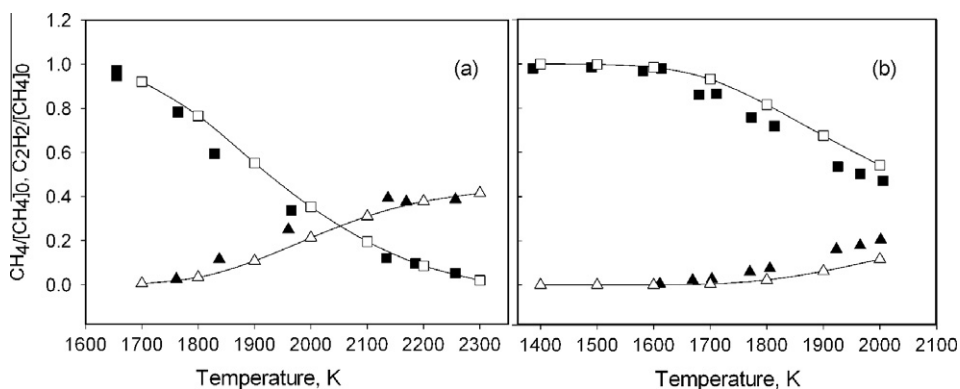


Fig. 2. Temperature dependences of the product yields for the shock-tube pyrolysis of (a)  $0.02 CH_4/Ar$  and (b)  $0.05 CH_4/Ar$  mixtures. Closed squares and triangles represent the measured concentrations of methane and acetylene, respectively [28]. Open symbols show the results of our calculations at  $p_{50} = 3.0$  bar for various temperatures and the corresponding reaction times (parenthesized, in ms) reported in [28]: (a) 1700 (1.94), 1800 (1.78), 1900 (1.62), 2000 (1.46), 2100 (1.30), 2200 (1.14), and 2300 K (1.00) and (b) 1400 (2.05), 1500 (1.90), 1600 (1.70), 1700 (1.62), 1800 (1.44), 1900 (1.24), and 2000 K (1.06).



the main species involved in propargyl  $C_3H_3$  formation. Propargyl radicals are the main contributors to the formation of a first aromatic ring (benzene  $C_6H_6$  (A1) molecules). A further growth of PAH molecules gives rise to soot precursors.

Figure 3 demonstrates good agreement between the experimentally measured in [40] and calculated product distributions in shock-tube pyrolysis of a  $0.016C_3H_8/Ar$  mixture.

The results of calculations were compared with our experimental measurements of soot formation in pyrolysis of various toluene/Ar mixtures (Fig. 4), an ethylbenzene/Ar mixture (Fig. 5), various benzene/Ar and benzene/ $O_2$ /Ar mixtures (Fig. 6), methane/Ar and methane/ $O_2$ /Ar

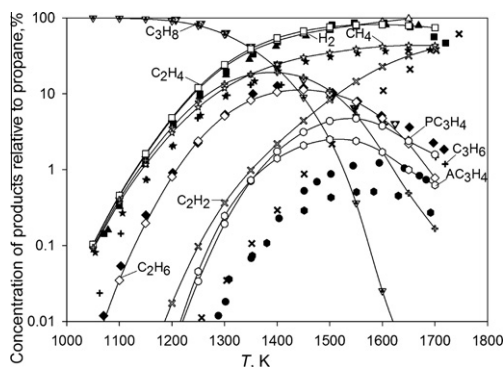


Fig. 3. Temperature dependences of the product yields for the shock-tube pyrolysis of a  $0.016 C_3H_8/Ar$  mixture ( $p_1 = 0.26$  bar,  $p_{50} = 7$  bar,  $\tau_{\text{reac}} = 1$  ms). The closed symbols show the experimental results [29], whereas the open symbols represent our calculation results.

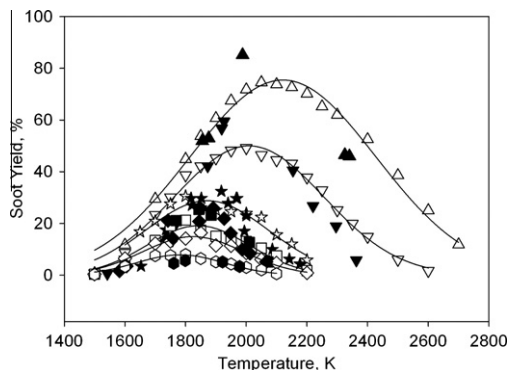


Fig. 4. Temperature dependences of the experimentally measured and calculated soot yields for various toluene/Ar mixtures: (triangles)  $0.9\%A1CH_3/Ar$ , (inverted triangles)  $0.5\%A1CH_3/Ar$ , (stars)  $0.25\%A1CH_3/Ar$ , (squares)  $0.17\%A1CH_3/Ar$ , (diamonds)  $0.15\%A1CH_3/Ar$ , (hexagons)  $0.097\%A1CH_3/Ar$ ,  $p_{50} = 3.0$  bar,  $\tau_{\text{reac}} = 1$  ms. The closed symbols represent our experimental results ( $E(m) = 0.37$ ), whereas the open symbols show calculation results.

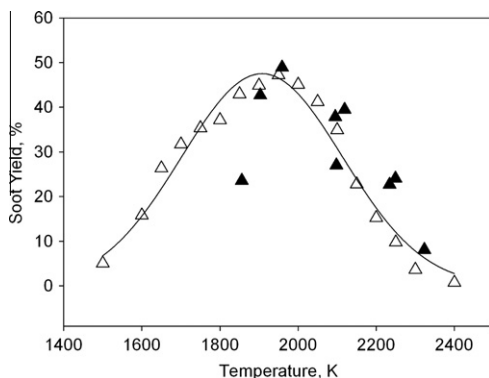


Fig. 5. Temperature dependences of the soot yield for the shock-tube pyrolysis of an ethylbenzene/Ar mixture:  $0.0033A1C_2H_5/Ar$ ,  $p_{50} = 3$  bar,  $\tau_{\text{reac}} = 1$  ms. The closed and open symbols represent our experimental and calculation results, respectively.

mixtures (Fig. 7), and different propane/Ar and propylene/Ar mixtures behind reflected shock waves. Benzene, toluene, and ethylbenzene demonstrate a good agreement between the experimentally measured and calculated temperature dependences of soot yield. Oxygen additives cause a rise in the temperature of test mixtures compared to oxygen-free mixtures, which, nevertheless remains lower than the calculated temperature behind the reflected shock wave. This leads to the shift of the maximum of soot yield toward the lower temperatures (Fig. 6).

As can be seen from Fig. 7, a good agreement between the experimentally measured and calculated soot yields is also observed for methane pyrolysis and oxidation. Oxygen additives significantly reduce the soot yield, and the maximum of the soot

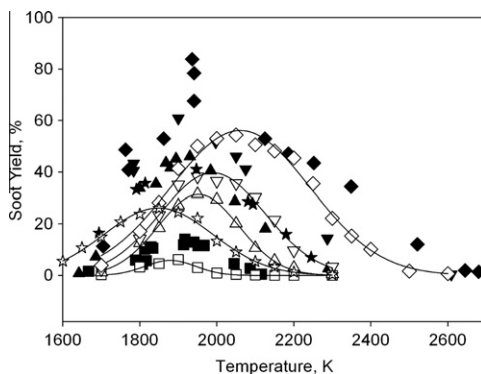


Fig. 6. Temperature dependences of the soot yield for the shock-tube pyrolysis of various benzene/Ar mixtures: (diamonds)  $0.01A1/Ar$ , (inverted triangles)  $0.0062A1/Ar$ , (triangles)  $0.00467A1/Ar$ , (squares)  $0.00175A1/Ar$ , and (stars)  $0.0062A1/0.005O_2/Ar$ ;  $p_{50} = 3$  bar,  $\tau_{\text{reac}} = 1$  ms. The closed and open symbols show our experimental and calculation results, respectively.

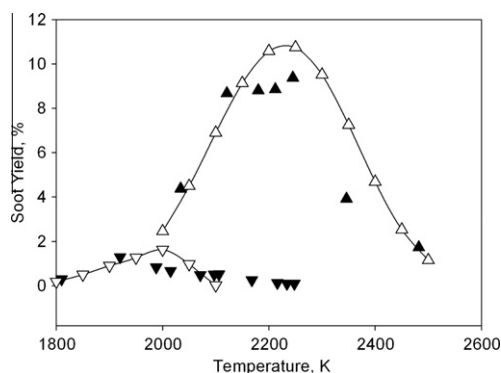


Fig. 7. Temperature dependences of the soot yield for the shock-tube pyrolysis of CH<sub>4</sub>/Ar and CH<sub>4</sub>/O<sub>2</sub>/Ar mixtures at  $p_{s0} = 5.0$  bar: 0.05CH<sub>4</sub>/Ar (triangles) and 0.05CH<sub>4</sub>/0.011O<sub>2</sub>/Ar (inverted triangles). The closed symbols designate our experimental data; the open symbols represent our calculation results ( $\tau_{\text{reac}} = 2$  ms).

yield temperature dependence shifts toward lower temperatures. This is associated with the oxidation of soot precursors and a temperature rise in the oxygen-containing mixtures behind reflected shock wave. In the case of propane and propylene pyrolysis, the agreement between experiments and calculations is satisfactory.

## 5. Conclusions

An extensive body of new experimental data on the characteristics of soot formation during the shock-tube pyrolysis and oxidation of a number of aromatic and aliphatic hydrocarbons was obtained, a set of measurements that required a thorough revision of our previous mechanism of soot formation. The proposed modified scheme was successfully tested by describing the temporal behavior of a number of key species during the primary stages of oxidation of various hydrocarbons under a variety of conditions. When applied to modeling our experimental data, it closely reproduced the time histories of the soot yield and temperature for the shock-tube pyrolysis of methane, propane, and propylene, as well as benzene, toluene, and ethylbenzene, two sets of compounds of drastically different natures.

The induction period of soot formation for aliphatic compounds was observed to be substantially longer than that for aromatic species, which can be explained by a longer pathway to the formation of soot nuclei, in agreement with the predictions of the kinetic mechanism.

The soot formation during the pyrolysis and oxidation of the hydrocarbons was demonstrated to be accompanied by a temperature drop, probably due to the predominance of decomposition stages; it was somewhat smaller in the case of oxi-

dative pyrolysis due to contributions from exothermic oxidation reactions.

## Acknowledgments

This work was supported by the Russian Foundation for Basic Research, Project No. 08-08-0722 and the Russia Federal Targeted Program “Research and Research-Human Resources for Innovating Russia”, Project NK-576P.

## Appendix A. Supplementary data

Supplementary data associated with this article can be found, in the online version, at [doi:10.1016/j.proci.2010.07.089](https://doi.org/10.1016/j.proci.2010.07.089).

## References

- [1] M. Frenklach, *Phys. Chem. Chem. Phys.* 4 (2002) 2028–2037.
- [2] R. Whitesides, M. Frenklach, *J. Phys. Chem. A* 114 (2010) 689–703.
- [3] A. D’Anna, in: H. Bockhorn, A. D’Anna, A.F. Sarofim, H. Wang (Eds.), *Combustion Generated Fine Carbonaceous Particles*, KIT Scientific Publishing, Karlsruhe Institut für Technologie, 2009, pp. 289–320.
- [4] A. D’Anna, A. Violi, A. D’Alessio, A.F. Sarofim, *Combust. Flame* 127 (2001) 1995–2003.
- [5] A. Violi, A.F. Sarofim, T.N. Truong, *Combust. Sci. Technol.* 174 (2002) 205–222.
- [6] A. Violi, *Combust. Flame* 139 (2004) 279–287.
- [7] S.H. Chung, A. Violi, in: H. Bockhorn, A. D’Anna, A.F. Sarofim, H. Wang (Eds.), *Combustion Generated Fine Carbonaceous Particles*, KIT Scientific Publishing, Karlsruhe Institut für Technologie, 2009, pp. 321–332.
- [8] B. Öktem, M.P. Tolocka, B. Zhao, H. Wang, M.V. Johnston, *Combust. Flame* 142 (2005) 364–373.
- [9] T.G. Baquet, H. Grotheer, M. Aigner, *Rapid Commun. Mass Spectrom.* 21 (2007) 4060–4064.
- [10] G.L. Agafonov, I. Naydenova, P.A. Vlasov, J. Warnatz, *Proc. Combust. Inst.* 31 (2007) 575–583.
- [11] G.L. Agafonov, A.A. Borisov, V.N. Smirnov, K.Ya. Troshin, P.A. Vlasov, J. Warnatz, *Combust. Sci. Technol.* 180 (10) (2008) 1876–1899.
- [12] G.L. Agafonov, I. Naydenova, V.N. Smirnov, et al., in: H. Bockhorn, A. D’Anna, A.F. Sarofim, H. Wang (Eds.), *Combustion Generated Fine Carbonaceous Particles*, KIT Scientific Publishing, Karlsruhe Institut für Technologie, 2009, pp. 385–404.
- [13] C. Schulz, B.F. Kock, M. Hofmann, et al., *Appl. Phys. B* 83 (2006) 333–354.
- [14] T.C. Williams, C.R. Shaddix, K.A. Jensen, J.M. Suo-Anttila, *Int. J. Heat Mass Transfer* 50 (2007) 1616–1630.
- [15] M. Frenklach, M.K. Ramachandra, R.A. Matula, *Proc. Combust. Inst.* 20 (1984) 871–878.
- [16] J. D’Alessio, M. Lazzaro, P. Massoli, V. Moccia, *Opt. Lasers Eng.* 37 (2002) 495–508.

- [17] H. Wang, X. You, A.V. Joshi, et al., USC Mech Version II, *High-Temperature Combustion Reaction Model of H<sub>2</sub>/CO/C1–C4 Compounds*, May 2007. Available at: <[http://ignis.usc.edu/USC\\_Mech\\_II.htm](http://ignis.usc.edu/USC_Mech_II.htm)>.
- [18] G. Blanquart, P. Pepiot-Desjardins, H. Pitsch, *Combust. Flame* 156 (2009) 588–607.
- [19] M. Frenklach, H. Wang, in: H. Bockhorn (Ed.), *Soot Formation in Combustion*, Springer-Verlag, Berlin, 1994, pp. 162–192.
- [20] S.J. Harris, A.M. Weiner, *Combust. Sci. Technol.* 31 (1983) 155–167.
- [21] J. Appel, H. Bockhorn, M. Frenklach, *Combust. Flame* 121 (1–2) (2000) 122–136.
- [22] P. Deuflhard, M. Wulkow, *Impact Comput. Sci. Eng.* 1 (1989) 269–301.
- [23] H. Richter, S. Granata, W.H. Green, J.B. Howard, *Proc. Combust. Inst.* 30 (2005) 1397–1405.
- [24] M.S. Skjøth-Rasmussen, P. Glarborg, M. Østberg, et al., *Combust. Flame* 136 (2004) 91–128.
- [25] C. Correa, H. Niemann, B. Schramm, J. Warnatz, *Proc. Combust. Inst.* 28 (2000) 1607–1614.
- [26] J. Huang, W.K. Bushe, *Combust. Flame* 144 (2006) 74–88.
- [27] H. Böhm, H. Jander, *Phys. Chem. Chem. Phys.* 1 (1999) 3775–3781.
- [28] P.A. Vlasov, J. Warnatz, *Proc. Combust. Inst.* 29 (2002) 2335–2341.
- [29] I. Naydenova, M. Nullmeier, J. Warnatz, P.A. Vlasov, *Combust. Sci. Technol.* 176 (2004) 1667–1703.
- [30] M. Frenklach, D.W. Clary, T. Yuan, W.C. Gardiner Jr., S.E. Stein, *Combust. Sci. Technol.* 50 (1986) 79–115.
- [31] M. Frenklach, J. Warnatz, *Combust. Sci. Technol.* 51 (1987) 265–283.
- [32] S. Scherer, *Untersuchung pyrolytischer Reaktionen des Rußvorläufermoleküls Propargyl im Stoßwellenrohr*, Ph.D. Thesis, Universität Stuttgart, Institut für Physikalische Chemie der Verbrennung des DLR in Stuttgart, 2001.
- [33] C. Horn, P. Frank, High Temperature Pyrolysis of Phenol, in: *Proc. Fourth Int. Conf. on Chemical Kinetics*, NIST, July 14–18, 1997, Gaithersburg, MD.
- [34] V. Vasudevan, D.F. Davidson, R.K. Hanson, *Proc. Combust. Inst.* 30 (2005) 1155–1163.
- [35] M.A. Oehlschlaeger, D.F. Davidson, R.K. Hanson, *J. Quant. Spectrosc. Radiat. Transfer* 92 (2005) 393–402.
- [36] R.D. Kern, H.J. Singh, M.A. Esslinger, P.W. Winkler, *Proc. Combust. Inst.* 19 (1982) 1351–1358.
- [37] R.D. Kern, C.H. Wu, G.B. Skinner, et al., *Proc. Combust. Inst.* 20 (1984) 789–797.
- [38] A. Laskin, A. Lifshitz, *Proc. Combust. Inst.* 26 (1996) 669–675.
- [39] Y. Hidaka, T. Nakamura, H. Tanaka, K. Inami, H. Kawano, *Int. J. Chem. Kinet.* 22 (1990) 701–709.
- [40] A. Lifshitz, M. Frenklach, *J. Phys. Chem.* 79 (7) (1975) 686–692.